

# Searching for isovector signatures in the neutron-rich oxygen and calcium isotopes

Wei-Chia Chen<sup>1,\*</sup> and J. Piekarewicz<sup>1,†</sup>

<sup>1</sup>*Department of Physics, Florida State University, Tallahassee, FL 32306*

(Dated: March 12, 2015)

We search for potential isovector signatures in the neutron-rich oxygen and calcium isotopes within the framework of a relativistic mean-field theory with an exact treatment of pairing correlations. To probe the isovector sector we calibrate a few relativistic density functionals using the same isoscalar constraints but with one differing isovector assumption. It is found that under certain conditions, the isotopic chain in oxygen can be made to terminate at the experimentally observed  $^{24}\text{O}$  isotope and in the case of the calcium isotopes at  $^{60}\text{Ca}$ . To produce such behavior, the resulting symmetry energy must be soft, with predicted values for the symmetry energy and its slope at saturation density being  $J = (30.92 \pm 0.47) \text{ MeV}$  and  $L = (51.0 \pm 1.5) \text{ MeV}$ , respectively. As a consequence, the neutron-skin thickness of  $^{208}\text{Pb}$  is rather small:  $R_{\text{skin}}^{208} = (0.161 \pm 0.011) \text{ fm}$ . This same model—labelled “*FSUGarnet*”—predicts  $R_{1.4} = (13.1 \pm 0.1) \text{ km}$  for the radius of a “canonical”  $1.4M_{\odot}$  neutron star, yet is also able to support a two-solar-mass neutron star.

PACS numbers: 21.60.Jz, 21.65.Cd, 21.65.Mn

Density functional theory (DFT) provides the only known tractable framework to describe strongly interacting nuclear many-body systems ranging from finite nuclei to neutron stars. In the spirit of DFT, the complicated many-body effects are implicitly encoded in the parameters of the model which in turn are determined by fitting directly to experimental data [1]. Thus, the quality of the resultant model depends not only on the form of the functional but, in addition, on the data used for its calibration. It is widely recognized that the isoscalar sector of the density functional is well constrained by available ground-state observables. This is in sharp contrast to the isovector sector that remains poorly determined; for a recent example see Ref. [2] and references contained therein. Such a mismatch occurs because physical observables that are dominated by the isoscalar sector—such as binding energies and charge radii of many stable nuclei—have been measured with enormous precision. Instead, data on neutron skins [3, 4] and neutron-star radii [5–8], both highly sensitive to the isovector sector, either lack precision or are still open to debate.

Due to the present difficulty in obtaining accurate measurements of both neutron skins and neutron-star radii, it seems prudent to seek alternative isovector indicators. A fruitful arena for the search of isovector sensitivity is pure neutron matter whose equation of state is approximately equal to that of symmetric nuclear matter plus the symmetry energy. The behavior of pure neutron matter at low densities is particularly attractive because of its close resemblance to a resonant Fermi gas. However, although this has stimulated significant amount of theoretical activity [9–16], one must recognize that neutron matter remains a purely theoretical construct. A laboratory observable that has been identified as a strong

isovector indicator is the electric dipole polarizability of  $^{208}\text{Pb}$  [17–20]. Indeed, the recent high-resolution measurement of the electric dipole polarizability of  $^{208}\text{Pb}$  at the Research Center for Nuclear Physics [21, 22] has provided a unique constraint on the density dependence of the symmetry energy and serves as an ideal complement to measurements of the neutron skin.

Given that the symmetry energy accounts for the energy cost in departing from equal number of protons and neutrons, one expects that the evolution of certain nuclear properties as one moves away from the valley of stability will become sensitive to the isovector nature of the interaction. For example, if the symmetry energy is *stiff*, namely, if it increases rapidly with density, it becomes energetically favorable to move neutrons from the core to the surface, resulting in a thick neutron skin [23]. By the same token, a stiff symmetry energy may become small at the dilute nuclear surface which is of particular relevance to the valence orbitals. As a result, a stiff symmetry energy predicts a delay in reaching the neutron drip line relative to their softer counterparts [24].

Mapping the precise boundaries of the nuclear landscape has been identified as one of the most fundamental problems in nuclear science; see Refs. [25, 26] and references contained therein. Although the proton drip line has been determined up to protactinium (atomic number  $Z=91$ ) the neutron drip line remains unknown, except in the case of a few light nuclei ( $Z \lesssim 8$ ) [27]. A particularly dramatic example of this mismatch is the case of the fluorine isotopes, which have  $^{19}\text{F}$  as its only stable member. Whereas  $^{17}\text{F}$  marks the boundary of the proton drip line,  $^{31}\text{F}$ —with 12 neutrons away from stability—remains stable against strong decays. While the Coulomb repulsion is largely responsible for having the proton drip line just a few neutrons away from stability, the basic tenet of this letter is that the dynamics of the neutron drip line is highly sensitive to the nuclear symmetry energy.

Among the few isotopic chains with both drip-line boundaries firmly established, oxygen is perhaps the

\*Electronic address: wc09c@my.fsu.edu

†Electronic address: jpiekarewicz@fsu.edu

most intriguing one, as it provides the first clear indication of the emergence of a new magic number at  $N=16$  [28]. Whereas most mean-field calculations (both non-relativistic and relativistic) have predicted the stability of the “doubly-magic” nucleus  $^{28}\text{O}$  against strong decays, experimental efforts have failed to find a stable isotope beyond  $^{24}\text{O}$  [28–31]. This *oxygen anomaly* has been widely investigated within various formulations and, to date, the most common explanation invokes an extra repulsion between valence neutrons generated from three-nucleon forces [32–37].

The calcium isotopic chain—the next chain after oxygen with a magic number of protons—has also received a great deal of attention due to its rich subshell structure near  $N=32$  [38–41]. Particularly exciting is the recent mass determination of various exotic calcium isotopes—up to  $^{54}\text{Ca}$ —at both TRIUMF [40] and CERN [41]. Yet, despite these remarkable achievements, the experimental determination of the neutron drip line in calcium is likely years away—especially if the drip line is at or beyond the “doubly-magic”  $^{60}\text{Ca}$ .

In order to explore the sensitivity of the neutron-rich isotopes to the density dependence of the symmetry energy, we construct theoretical models subject to the same isoscalar constraints but with a single differing assumption on the uncertain isovector sector. In the relativistic mean-field (RMF) theory, the nuclear system is composed of neutrons and protons interacting via the exchange of various mesons and the photon. In the version of the RMF models employed here the interaction among the particles is described by an effective Lagrangian density [42–44] whose parameters are determined by fitting model predictions to experimental data. In this work we employ the Lagrangian density given in Ref. [2] and use the same calibration scheme developed therein to find the optimal model parameters and their associated theoretical uncertainties [45]. Such a fitting protocol relies exclusively on genuine physical observables that can be either measured in the laboratory or extracted from observation. This approach was recently implemented in building the new *FSUGold2* density functional [2]. The data pool of observables is sufficient to constrain the isoscalar sector as evinced by the very small associated theoretical uncertainties. However, because no inherent isovector biases are incorporated into the fit, *FSUGold2* predicts—in accordance with most relativistic density functionals—a stiff symmetry energy and, as a consequence, a fairly thick neutron skin in  $^{208}\text{Pb}$  of  $R_{\text{skin}}^{208} = (0.287 \pm 0.020)$  fm. In an effort to explore the sensitivity of the isovector sector to the mass evolution along the isotopic chains in oxygen and calcium, we now tune the density dependence of the symmetry energy by adding into the calibration an assumed value for the neutron-skin thickness of  $^{208}\text{Pb}$ . That is, we augment the calibration procedure by assuming values of  $R_{\text{skin}}^{208} = 0.12$  fm,  $R_{\text{skin}}^{208} = 0.16$  fm, and  $R_{\text{skin}}^{208} = 0.28$  fm—in all three cases with an associated error of 0.2%. For simplicity, the resulting relativistic mean-field models are labeled by their assumed value of

$R_{\text{skin}}^{208}$ , namely, RMF012, RMF016, and RMF028. Given that the data pool of observables involves doubly-magic (or semi-magic) nuclei, pairing correlations are not included in the calibration procedure. However, once the calibration is completed, we exploit our recently developed RMF-plus-exact-pairing (RMF+EP) approach [46] to properly describe the mass evolution along both isotopic chains.

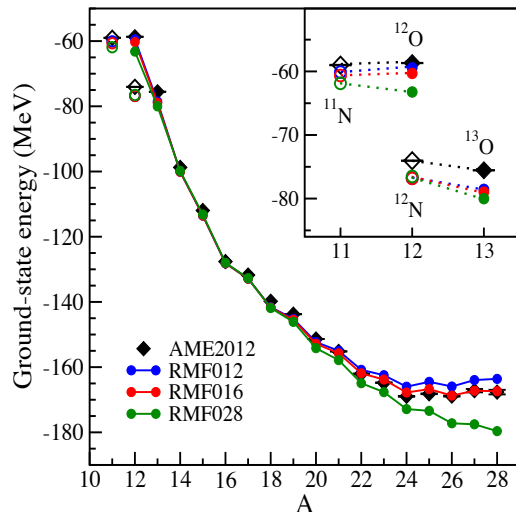


FIG. 1: (Color online). Evolution of the ground-state energy along the isotopic chain in oxygen—from  $^{12}\text{O}$  to  $^{28}\text{O}$ —as predicted by the three RMF models described in the text. Experimental data are from Ref. [47].

We start by displaying in Fig. 1 the evolution of the ground-state energy along the isotopic chain in oxygen. Given that the nearly isospin-symmetric isotopes  $^{14}$ – $^{18}\text{O}$  are largely insensitive to the isovector sector, the model predictions are almost indistinguishable from each other and are also in good agreement with the 2012 Atomic Mass Evaluation (AME2012) [47]. However, as the neutron-proton asymmetry is increased, the model predictions start to differ, indicating that isovector effects are starting to play an increasingly dominant role. Indeed, the models display dramatic differences as the experimentally determined neutron drip line at  $^{24}\text{O}$  is approached. Although drip-line nuclei are undoubtedly sensitive to subtle dynamical effects, e.g., mixing to the continuum, it appears that the density dependence of the symmetry energy also plays a critical role. In particular, we find that RMF028 (with the stiffest symmetry energy) overbinds the neutron-rich isotopes, leading to the common, yet erroneous, prediction of a drip line at  $^{28}\text{O}$ . In contrast, RMF012 and RMF016 with a softer symmetry energy produce the necessary *repulsion* to shift the neutron drip line to  $^{24}\text{O}$ . We must underline that such behavior is determined by the weakly-bound excess neutrons that reside in the nuclear surface where the density is low. Thus, it is the low-density component of the symmetry energy—which is *larger* for a soft model—

that dictates the physics, rather than the symmetry energy around saturation density. This suggests that models with a small  $R_{\text{skin}}^{208}$  should be the first ones to reach the neutron drip line [24], precisely as seen in Fig. 1. Although Coulomb effects shift the proton drip line much closer to stability, the imprint of the symmetry energy should also be manifest on the neutron-deficient side of the isotopic chain. Indeed, this appears to be the case. As highlighted in the inset of Fig. 1, both RMF012 and RMF016 predict—unlike RMF028—that  $^{12}\text{O}$  is unstable against proton emission, in agreement with experiment. Thus, as in the case of the neutron drip line, the two softer models reach the proton drip line earlier than the stiffer one. Note that the true ground state of the odd-odd nucleus  $^{12}\text{N}$  is a superposition of states with the unpaired proton and neutron being in orbitals that can couple to the ground-state spin of the nucleus (i.e.,  $J^\pi = 1^+$ ). However, for simplicity we approximate the ground-state energy of  $^{12}\text{N}$  by the lowest-energy configuration. The inset on Fig. 1 seems to validate this approximation.

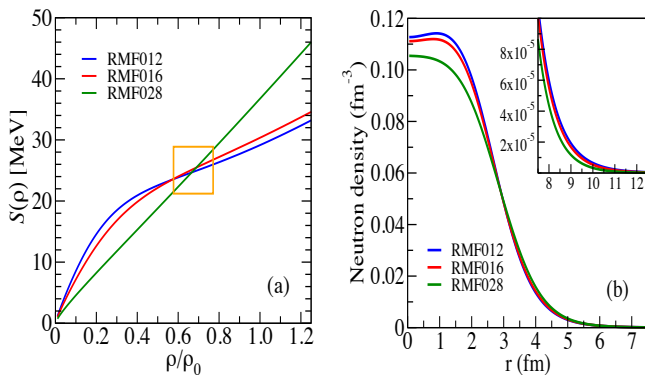


FIG. 2: (Color online). (a) Symmetry energy as a function of density in units of  $\rho_0 = 0.148 \text{ fm}^{-3}$  and (b) neutron density of  $^{24}\text{O}$  as predicted by the three RMF models discussed in the text.

To further validate this behavior, we display in Fig. 2a the symmetry energy predicted by the three models up to a density slightly above saturation density. The thickness of the neutron skin in  $^{208}\text{Pb}$  is largely determined by the *slope* of the symmetry energy at (or near) saturation density. In the case of a stiff symmetry energy, such as RMF028, it is energetically advantageous to move neutrons from the core (where  $S$  is large) to the surface (where  $S$  is small), albeit at the expense of an increase in surface tension. Thus, models with a stiff symmetry energy tend to predict thicker neutron skins. However, at a density of about 2/3 of saturation density, corresponding to a value of the symmetry energy of almost 26 MeV, all three models intersect each other. This well-known result emerges from the sensitivity of the binding energy of neutron-rich nuclei to the symmetry energy at a density that is intermediate between that of the core and the surface [23, 44, 48–52]. As a result, the symmetry energy below this density becomes larger for the softer models. This increase in the symmetry energy generates

the added repulsion required to shift the neutron drip line from  $^{28}\text{O}$  to  $^{24}\text{O}$ .

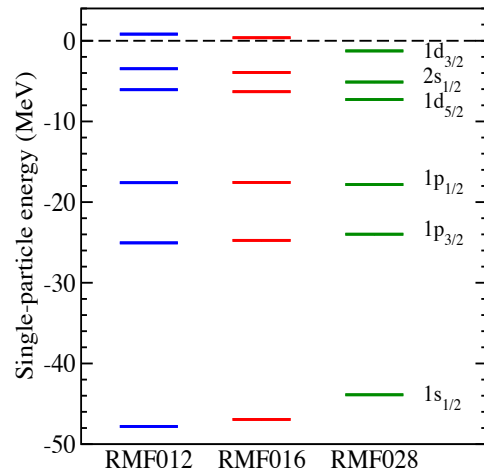


FIG. 3: (Color online). Single-neutron spectrum for  $^{24}\text{O}$  as predicted by the three RMF models discussed in the text.

Such unique behavior of the symmetry energy leaves a distinct imprint on the neutron density of  $^{24}\text{O}$ ; see Fig. 2b. First, we note that for a stiff symmetry energy, as in the case of RMF028, more neutrons are pushed to the surface resulting in both a depletion of the density in the interior and a larger neutron radius. Second, at a distance of about 3 fm, corresponding to a density of about  $0.05 \text{ fm}^{-3}$ , the neutron density predicted by the RMF028 model now becomes the largest, as this is the region that dominates the contribution to the neutron radius. Finally, at even larger distances where the density is dominated by the weakly-bound valence neutrons, the density is again lowest for the stiffest model (see the inset in Fig. 2b). That is, the smaller symmetry energy at low density of the RMF028 model yields less repulsion for the valence orbitals and consequently a faster falloff of the density. The single-neutron spectrum displayed in Fig. 3 serves to reaffirm these trends. In particular, we notice a “compression” of the single-particle spectrum as the symmetry energy becomes stiffer. Indeed, whereas the “core”  $sp$ -orbitals become less bound with increasing stiffness, the valence  $sd$ -orbitals are more strongly bound. Particularly, the neutron  $1d_{3/2}$  orbital becomes unbound for the softer models—a critical requirement for the drip line in oxygen to be found at  $^{24}\text{O}$ .

We continue by displaying in Fig. 4 ground-state energies for calcium—the next isotope with a fully closed proton shell. Predictions have been made for a wide range of neutron-proton asymmetries starting with  $^{33}\text{Ca}$  and ending with the very neutron-rich  $^{70}\text{Ca}$  isotope. The calculation for the neutron-rich isotopes was done using the augmented  $fp g_{9/2}$  valence space. It is found that including the  $1g_{9/2}$  orbital enhances the binding energy in the  $^{40-60}\text{Ca}$  region bringing the predictions from both RMF012 and RMF016 into closer agreement with exper-

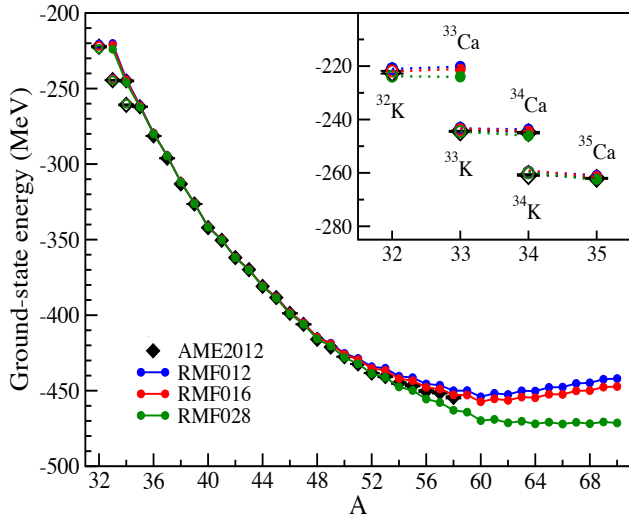


FIG. 4: (Color online). Evolution of the ground-state energy along the isotopic chain in calcium—from  $^{33}\text{Ca}$  to  $^{70}\text{Ca}$ —as predicted by the three RMF models described in the text. Experimental data are from Ref. [47].

iment. Also shown in the figure are experimental data from the latest AME2012 compilation [47]. Note that the AME2012 results quoted for  $^{53}\text{Ca}$  and beyond were “derived not from purely experimental data” [47]. Contrary to the isotopic chain in oxygen where the neutron drip line has been firmly established, the experimental data show no evidence that the neutron drip line is within reach. Given that all three models were calibrated using ground-state energies for both  $^{40}\text{Ca}$  and  $^{48}\text{Ca}$ , it is not surprising that the agreement among them—and with experiment—is very good. However, beyond  $^{48}\text{Ca}$  where isovector effects start to play a critical role, significant differences emerge. In particular, and fully consistent with the results obtained along the isotopic chain in oxygen, the stiff RMF028 model predicts an overbinding that is inconsistent with experiment. Although all three models agree that  $^{60}\text{Ca}$  is particle bound, a subtle odd-even staggering emerges thereafter. Nevertheless, upon closer examination we found that for RMF012 and RMF016 the neutron drip line is reached at  $^{60}\text{Ca}$ . On the other hand, the very flat plateau displayed by RMF028 makes it difficult to identify the exact location of the neutron drip line. This observation is also supported by the single-neutron energies of  $^{60}\text{Ca}$  displayed in Fig. 5. Indeed, compared to its softer counterparts, the barely unbound  $1g_{9/2}$  orbital in RMF028 makes the identification of the drip line ambiguous. We stress that a more accurate description of the neutron drip line remains a serious theoretical challenge. For example, whereas Holt and collaborators [38] predict—like we do—that the neutron drip line will be reached at or beyond  $^{60}\text{Ca}$ , Hagen *et al.* find  $^{60}\text{Ca}$  to be particle unbound relative to  $^{56}\text{Ca}$  [39]. However, while the results of Holt *et al.* depend critically on the role of three-nucleon forces, Ekström and collaborators have

recently found that a properly optimized chiral nucleon-nucleon interaction can describe many aspects of nuclear structure without explicitly invoking three-nucleon forces [53].

Finally, we turn to the neutron-deficient side of the calcium isotopes. As shown in Fig. 4 and highlighted in the inset, models with a soft symmetry energy reach both drip lines earlier than their stiffer counterparts. Indeed, whereas the proton drip line in both RMF012 and RMF016 can be placed at  $^{34}\text{Ca}$  in agreement with experiment, RMF028 predicts its location at or beyond  $^{33}\text{Ca}$ . (Again, for the odd-odd nuclei,  $^{32}\text{K}$  and  $^{34}\text{K}$ , we used the same approximation as for  $^{12}\text{N}$ .)

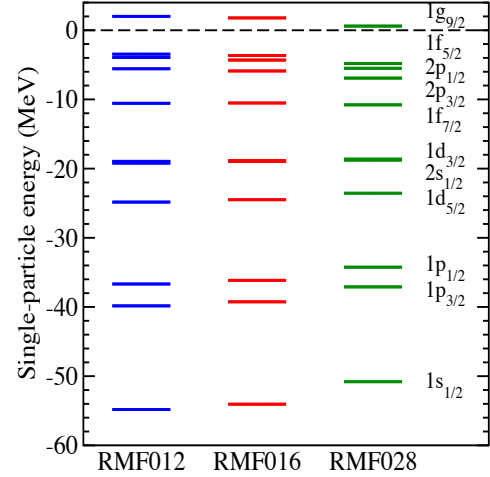


FIG. 5: (Color online). Single-neutron spectrum for  $^{60}\text{Ca}$  as predicted by the three RMF models discussed in the text. Note that the  $2s_{1/2}$  and  $1d_{3/2}$  orbitals are predicted to be nearly degenerate in all three models.

The results obtained so far suggest that by adopting certain reasonable assumptions one can reproduce the observed experimental trends in the isotopic chains of both oxygen and calcium. In our particular case, such a “plausible assumption” implies the adoption of an ad-hoc value of  $R_{\text{skin}}^{208}$ . This finding is significant as it has been previously shown that calibrating RMF functionals by relying exclusively on well-measured physical observables invariably results in the prediction of fairly large neutron skins [2, 45, 54]. Instead, one immediate consequence of the present analysis is that the neutron-skin thickness of neutron-rich nuclei can not be overly large. Indeed, the model that can best reproduce ground-state energies along the oxygen and calcium isotopic chains is RMF016—a model that henceforth will be referred to as “*FSUGarnet*”. This model predicts  $R_{\text{skin}}^{208} = (0.161 \pm 0.011) \text{ fm}$ . In turn, the strong correlation between  $R_{\text{skin}}^{208}$  and neutron-star radii leads to the following prediction for the radius of a  $1.4M_{\odot}$  neutron star:  $R_{1.4} = (13.1 \pm 0.1) \text{ km}$ . Note that although the symmetry energy is relatively soft, the overall equation of state is stiff enough to support a two-solar-mass neutron star [55, 56]. Indeed, the maximum neutron-star mass

supported by FSUGarnet is  $M_{\max} = (2.07 \pm 0.02) M_{\odot}$ . Finally, given that no property of infinite nuclear matter was incorporated into the fit, the symmetry energy  $J = (30.92 \pm 0.47)$  MeV and its slope  $L = (51.0 \pm 1.5)$  MeV at saturation density represent legitimate model predictions.

Although all our results were obtained from the calibration of a relativistic density functional constrained exclusively from experimental and observational data—plus a critical assumption on  $R_{\text{skin}}^{208}$ —it is instructive to compare them against the predictions from various other analyses. In the particular case of the neutron-skin thickness of  $^{208}\text{Pb}$ , it falls safely within the  $R_{\text{skin}}^{208} = (0.14 - 0.23)$  fm range suggested by a myriad of different analyses [21, 57–64]. In regard to the symmetry energy and its slope at saturation density, many of these same publications are consistent with the predictions from FSUGarnet. This is not overly surprising given that the value of the symmetry energy  $J$  is largely constrained by nuclear masses and its slope  $L$  by the value of  $R_{\text{skin}}^{208}$ .

In summary, we have explored sensitivity to isovector effects in the neutron-rich oxygen and calcium isotopes by calibrating RMF models with the same isoscalar constraints but with a single differing assumption on the

isovector sector: the neutron-skin thickness of  $^{208}\text{Pb}$ . We found that in these neutron-rich isotopes isovector effects play a critical role in reproducing the correct experimental trends along both isotopic chains. In particular, FSUGarnet—a newly calibrated relativistic density functional—displays a soft symmetry energy that can provide the extra repulsion required to terminate the oxygen chain at  $^{24}\text{O}$  and predicts the neutron drip line in calcium to be reached at  $^{60}\text{Ca}$ . The same isovector trends were also found on the neutron-deficient side of both isotopic chains. Indeed, FSUGarnet predicts the proton drip line in oxygen and calcium to be reached at  $^{13}\text{O}$  and  $^{34}\text{Ca}$ , in agreement with experiment. Although we have established the critical role that the symmetry energy plays in the delineation of the drip lines, we recognize that our results may be model dependent (see Ref. [65]). Yet, we are confident that our findings are of sufficient interest to motivate alternative studies with other classes of density functionals.

This material is based upon work supported by the U.S. Department of Energy Office of Science, Office of Nuclear Physics under Award Number DE-FD05-92ER40750.

- 
- [1] W. Kohn, *Rev. Mod. Phys.* **71**, 1253 (1999).
  - [2] W.-C. Chen and J. Piekarewicz, *Phys. Rev. C* **90**, 044305 (2014).
  - [3] S. Abrahamyan, Z. Ahmed, H. Albataineh, K. Aniol, D. Armstrong, et al., *Phys. Rev. Lett.* **108**, 112502 (2012).
  - [4] C. Horowitz, Z. Ahmed, C. Jen, A. Rakhman, P. Souder, et al., *Phys. Rev. C* **85**, 032501 (2012).
  - [5] F. Ozel, G. Baym, and T. Guver, *Phys. Rev. D* **82**, 101301 (2010).
  - [6] A. W. Steiner, J. M. Lattimer, and E. F. Brown, *Astrophys. J.* **722**, 33 (2010).
  - [7] V. Suleimanov, J. Poutanen, M. Revnivtsev, and K. Werner, *Astrophys. J.* **742**, 122 (2011).
  - [8] S. Guillot, M. Servillat, N. A. Webb, and R. E. Rutledge, *Astrophys. J.* **772**, 7 (2013).
  - [9] A. Schwenk and C. J. Pethick, *Phys. Rev. Lett.* **95**, 160401 (2005).
  - [10] A. Gezerlis and J. Carlson, *Phys. Rev. C* **81**, 025803 (2010).
  - [11] I. Vidaña, C. Providencia, A. Polls, and A. Rios, *Phys. Rev. C* **80**, 045806 (2009).
  - [12] S. Gandolfi, A. Y. Illarionov, K. Schmidt, F. Pedrera, and S. Fantoni, *Phys. Rev. C* **79**, 054005 (2009), 0903.2610.
  - [13] K. Hebeler and A. Schwenk, *Phys. Rev. C* **82**, 014314 (2010).
  - [14] I. Tews, T. Krüger, K. Hebeler, and A. Schwenk, *Phys. Rev. Lett.* **110**, 032504 (2013).
  - [15] T. Krüger, I. Tews, K. Hebeler, and A. Schwenk, *Phys. Rev. C* **88**, 025802 (2013).
  - [16] S. Gandolfi, J. Carlson, S. Reddy, A. Steiner, and R. Wiringa, *Eur. Phys. J. A* **50**, 10 (2014).
  - [17] P.-G. Reinhard and W. Nazarewicz, *Phys. Rev. C* **81**, 051303 (2010).
  - [18] J. Piekarewicz, *Phys. Rev. C* **83**, 034319 (2011).
  - [19] J. Piekarewicz, B. Agrawal, G. Colò, W. Nazarewicz, N. Paar, et al., *Phys. Rev. C* **85**, 041302(R) (2012).
  - [20] X. Roca-Maza, M. Centelles, X. Viñas, M. Brenna, G. Colò, et al., *Phys. Rev. C* **88**, 024316 (2013).
  - [21] A. Tamii et al., *Phys. Rev. Lett.* **107**, 062502 (2011).
  - [22] I. Poltoratska, P. von Neumann-Cosel, A. Tamii, T. Adachi, C. Bertulani, et al., *Phys. Rev. C* **85**, 041304 (2012).
  - [23] C. Horowitz, E. Brown, Y. Kim, W. Lynch, R. Michaels, et al., *J. Phys. G* **41**, 093001 (2014).
  - [24] B. G. Todd and J. Piekarewicz, *Phys. Rev. C* **67**, 044317 (2003).
  - [25] J. Erler, N. Birge, M. Kortelainen, W. Nazarewicz, E. Olsen, et al., *Nature* **486**, 509 (2012).
  - [26] A. V. Afanasjev, S. E. Agbemava, D. Ray, and P. Ring, *Phys. Lett. B* **726**, 680 (2013).
  - [27] M. Thoennessen, *Rep. Prog. Phys.* **67**, 1187 (2004).
  - [28] C. Hoffman, T. Baumann, D. Bazin, J. Brown, G. Christian, et al., *Phys. Lett. B* **672**, 17 (2009).
  - [29] M. Langevin et al., *Phys. Lett. B* **150**, 71 (1985).
  - [30] D. Guillemaud-Mueller et al., *Phys. Rev. C* **41**, 937 (1990).
  - [31] M. Fauerbach et al., *Phys. Rev. C* **53**, 647 (1996).
  - [32] T. Otsuka, T. Suzuki, J. D. Holt, A. Schwenk, and Y. Akaishi, *Phys. Rev. Lett.* **105**, 032501 (2010).
  - [33] G. Hagen, M. Hjorth-Jensen, G. R. Jansen, R. Machleidt, and T. Papenbrock, *Phys. Rev. Lett.* **108**, 242501 (2012).
  - [34] H. Hergert, S. Binder, A. Calci, J. Langhammer, and R. Roth, *Phys. Rev. Lett.* **110**, 242501 (2013).
  - [35] A. Cipollone, C. Barbieri, and P. Navrátil, *Phys. Rev.*

- Lett. **111**, 062501 (2013).
- [36] S. K. Bogner, H. Hergert, J. D. Holt, A. Schwenk, S. Binder, et al., Phys. Rev. Lett. **113**, 142501 (2014).
  - [37] G. R. Jansen, J. Engel, G. Hagen, P. Navratil, and A. Signoracci, Phys. Rev. Lett. **113**, 142502 (2014).
  - [38] J. D. Holt, T. Otsuka, A. Schwenk, and T. Suzuki, J. Phys. G **39**, 085111 (2012).
  - [39] G. Hagen, M. Hjorth-Jensen, G. R. Jansen, R. Machleidt, and T. Papenbrock, Phys. Rev. Lett. **109**, 032502 (2012).
  - [40] A. Gallant, J. Bale, T. Brunner, U. Chowdhury, S. Ettenauer, et al., Phys. Rev. Lett. **109**, 032506 (2012).
  - [41] F. Wienholtz, D. Beck, K. Blaum, C. Borgmann, M. Breitenfeldt, et al., Nature **498**, 346 (2013).
  - [42] H. Mueller and B. D. Serot, Nucl. Phys. A **606**, 508 (1996).
  - [43] B. D. Serot and J. D. Walecka, Int. J. Mod. Phys. E **6**, 515 (1997).
  - [44] C. J. Horowitz and J. Piekarewicz, Phys. Rev. Lett. **86**, 5647 (2001).
  - [45] J. Piekarewicz, W.-C. Chen, and F. J. Fattoyev, J. Phys. G **42**, 034018 (2015).
  - [46] W.-C. Chen, J. Piekarewicz, and A. Volya, Phys. Rev. C **89**, 014321 (2014).
  - [47] M. Wang, G. Audi, A. H. Wapstra, F. G. Kondev, M. MacCormick, X. Xu, and B. Pfeiffer, Chin. Phys. C **36**, 1603 (2012).
  - [48] M. Farine, J. Pearson, and B. Rouben, Nucl. Phys. A **304**, 317 (1978).
  - [49] B. A. Brown, Phys. Rev. Lett. **85**, 5296 (2000).
  - [50] R. J. Furnstahl, Nucl. Phys. A **706**, 85 (2002).
  - [51] B. A. Brown, Phys. Rev. Lett. **111**, 232502 (2013).
  - [52] Z. Zhang and L.-W. Chen, Phys. Lett. B **726**, 234 (2013).
  - [53] A. Ekstrom, G. Baardsen, C. Forssen, G. Hagen, M. Hjorth-Jensen, et al., Phys. Rev. Lett. **110**, 192502 (2013).
  - [54] F. Fattoyev and J. Piekarewicz, Phys. Rev. Lett. **111**, 162501 (2013).
  - [55] P. Demorest, T. Pennucci, S. Ransom, M. Roberts, and J. Hessels, Nature **467**, 1081 (2010).
  - [56] J. Antoniadis, P. C. Freire, N. Wex, T. M. Tauris, R. S. Lynch, et al., Science **340**, 1233232 (2013).
  - [57] A. Carbone, G. Colò, A. Bracco, L.-G. Cao, P. F. Bortignon, F. Camera, and O. Wieland, Phys. Rev. C **81**, 041301 (2010).
  - [58] K. Hebeler, J. M. Lattimer, C. J. Pethick, and A. Schwenk, Phys. Rev. Lett. **105**, 161102 (2010).
  - [59] P. Moller, W. D. Myers, H. Sagawa, and S. Yoshida, Phys. Rev. Lett. **108**, 052501 (2012).
  - [60] A. W. Steiner and S. Gandolfi, Phys. Rev. Lett. **108**, 081102 (2012).
  - [61] M. B. Tsang et al., Phys. Rev. C **86**, 015803 (2012).
  - [62] J. M. Lattimer, Annu. Rev. Nucl. Part. Sci. **62**, 485 (2012).
  - [63] K. Hebeler, J. M. Lattimer, C. J. Pethick, and A. Schwenk, Astrophys. J. **773**, 11 (2013).
  - [64] J. M. Lattimer and Y. Lim, Astrophys. J. **771**, 51 (2013).
  - [65] G. Co, V. De Donno, P. Finelli, M. Grasso, M. Anguiano, A. M. Lallena, C. Giusti, A. Meucci, and F. D. Pacati, Phys. Rev. C **85**, 024322 (2012).